Inorganic Chemistry

COMMUNICATION

pubs.acs.org/IC

Buckled Layers in $K_{0.66}Mn_2O_4 \cdot 0.28H_2O$ and $K_{0.99}Mn_3O_6 \cdot 1.25H_2O$ Synthesized at High Pressure: Implication for the Mechanism of Layer-to-Tunnel Transformation in Manganese Oxides

Qingxin Chu, Xiaofeng Wang, Xinhao Zhang, Qiliang Li, and Xiaoyang Liu*

State Key Laboratory of Inorganic Synthesis and Preparative Chemistry, Jilin University, Changchun 130012, China

Supporting Information

ABSTRACT: A 2 × 2 layer-buckled manganese oxide, $K_{0.66}Mn_2O_4 \cdot 0.28H_2O$ (**I**), has been synthesized under high pressure and retained at ambient pressure; it is metastable and will finally transform to a 2 × 1 layer-buckled $K_{0.99}Mn_3O_6 \cdot 1.25H_2O$ (**II**) in 1 year. Both crystal structures were determined by single-crystal X-ray diffraction. On the basis of these buckled layers, which are a result of ordering of Mn^{3+}/Mn^{4+} in separate rows and cooperative Jahn−Teller distortion of $Mn^{3+}O_6$ octahedra, a mechanism of structure transformation from birnessite to tunnel structures was proposed.

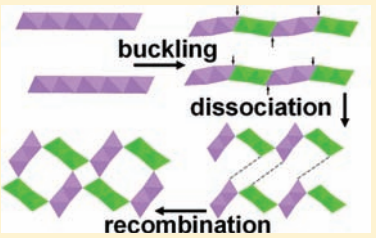

Unexpected fascinating phases may appear when nanoporous materials are subjected to high pressure (HP) because HP affects not only the structure of the flexible open framework but also the fate of extraframework cations and the guest molecules in the nanopores, resulting in volume contraction or expansion.[1−4] The layered structures, such as graphite oxide (GO), have attracted considerable interest because of their ability to accommodate different solvents under HP. GO layers are buckled, deviating from the ideal planar shape at the positions of functional group bonding.[1] Birnessite-related materials present similar layered structures, and the MnO_6 octahedral layers may also be buckled because of the mixed-valent MnO_6 octahedral layer of Mn^{3+}/Mn^{4+} with a distinct steric environment,[5] which is expected to be magnified under HP.[6] Because it is usually difficult to grow large enough crystals for a single-crystal X-ray diffraction (XRD) study, to date, however, structure models of birnessite determined from powder XRD show us only a simple planar MnO_6 layer.[5,7] In this study, HP not only can enhance the crystallinity and crystal size of birnessite but also can force Mn^{3+} and Mn^{4+} into an ordered state by elongation and orientation of the $Mn^{3+}O_6$ octahedra. A 2 × 2 buckled MnO_6 octahedral layer of $K_{0.66}Mn_2O_4 \cdot 0.28H_2O$ (**I**) was stabilized at HP (50 MPa) and transformed to a 2 × 1 buckled MnO_6 octahedral layer of $K_{0.99}Mn_3O_6 \cdot 1.25H_2O$ (**II**) when annealed at room temperature in air for 1 year. Both structures were determined by single-crystal XRD.

Birnessite is a layered mixed-valent manganese oxide built from edge-sharing MnO_6 octahedra with Na^+, K^+, or other cations and water molecules filling the interlayer space.[7] Its interlayer spacing is about 7 Å and can be tuned by incorporation of different species, such as metallic cations, oxides, organic molecules, etc.[8−11] Thus, it can be exploited in the fabrication of electrodes, catalysts, ion sieves, and adsorbents.[8,12−16] It is usually observed as an intermediate or used as a precursor in the synthesis of tunnel structures.[13,17] However, the intrinsic mechanism of layer-to-tunnel transformation has not yet been clear. Silvester et al. have studied the conversion of synthetic Na-rich buserite to hexagonal H^+-exchanged birnessite at low pH and found that the process starts with a disproportionation reaction of neighboring Mn^{3+} ions in the manganese oxide layers to Mn^{4+} and Mn^{2+} ions. The Mn^{2+} ions migrate into the interlayer space, undergo further oxidation to Mn^{3+} by oxygen, and assist the formation of corner-sharing MnO_6 octahedra.[18] However, the transformations in alkaline conditions or solid-state reactions are obviously different because there is nearly no soluble Mn^{2+}. In this work, a HP flux method [see the Supporting Information (SI) for synthesis details] was used to synthesize a layered manganese oxide, **I**, which shows us a new implication for the layer-to-tunnel transformation in manganese oxides.

The crystal structure of **I**[19] is very similar to that of birnessite synthesized in alkaline conditions.[7] Previous studies on powder XRD suggested that the octahedral layer in birnessite is an ideal plane.[7] However, the octahedral layer in this work is obviously buckled along the *c* axis (Figure 1a). As a result, Mn ions fall into two types, Mn(1) and Mn(2). Edge-sharing $Mn(1)O_6$ and $Mn(2)O_6$ octahedral dimers connect alternately by edges along the *c* axis and pack along the *b* axis to form MnO_6 layers. This is defined as a 2 × 2 buckle, referring to the definition of tunnel manganese oxides.[13] Because Mn^{3+} is a Jahn−Teller active ion with a larger radius than Mn^{4+}, Mn^{3+} and Mn^{4+} have the tendency to occupy Mn(2) and Mn(1) sites, respectively, because the $Mn(2)O_6$ octahedron is no doubt elongated at the apical direction (Figures 1a and 2a). These results agree well with the proposed arrangement of Mn^{3+} and Mn^{4+} in separate rows in birnessite based on extended X-ray absorption fine structure (EXAFS) analysis.[18,20] The layers are superimposed along the [110] direction, and K^+ ions deviate from the edges of the prisms (Figure S6 in the SI) compared with K-birnessite (Figure S2 in

Received: November 13, 2010
Published: January 26, 2011

dx.doi.org/10.1021/ic102282v | *Inorg. Chem.* 2011, 50, 2049–2051

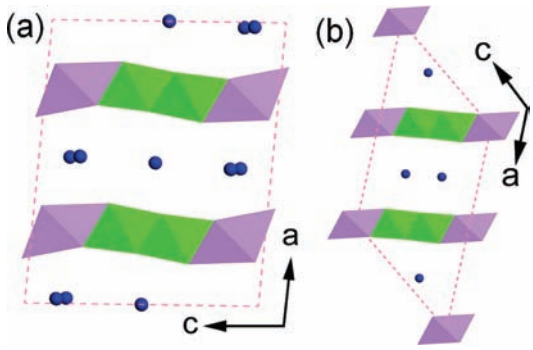

Figure 1. Crystal structures of **I** (a) and **II** (b) looking down the *b* axis, respectively. Green, purple, and blue represent Mn(1), Mn(2), and K/H_2O, respectively.

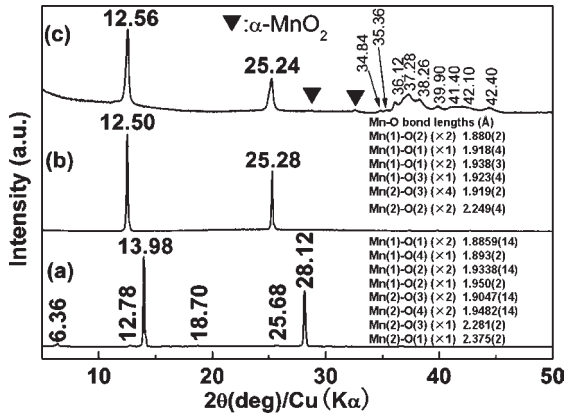

Figure 2. XRD patterns of **I** (a), **II** (b), and synthetic K-birnessite (c), respectively. (Insets a and b show the selected bond lengths for **I** and **II** in angstroms, respectively.)

the SI).[7] The basal plane distance of **I** is about 6.38 Å (half of the *a* value), corresponding to a featured XRD peak of **I** at 13.98° (Figure 2a), comparable to previously reported 6.44 Å for dehydrated K-birnessite.[15] The weak peak at 12.78° (25.68°) of **I**, which indicates that there are small amounts of water molecules between the layers, is shifted to a higher angle compared with 12.56° (25.24°) of synthetic birnessite (synthesized in hydrothermal conditions; see the SI) and 12.50° (25.28°) of **II** (Figure 2b, c), suggesting a strong interaction between water molecules and the MnO_6 octahedral layers. Thermogravimetric analysis (TGA) indicates that the water content is about 2.5% (Figure S9 in the SI). Therefore, the obtained structure of **I** is an average structure, which neglects those interlayered water molecules. Other weak peaks at 6.36° and 18.70° of **I** indicate that the initial structure is changed a little by the interlayered water molecules (Figure S7 in the SI), and both will finally disappear (Figures 2b and S4 in the SI) when **I** is annealed at room temperature in air. **I** will gradually relieve the lattice strain (see the Raman study below) and finally transform to birnessite in 1 month (Figure S3 in the SI). In this process, the positions and intensities of most Bragg diffractions are changed all of the time (Figure S4 in the SI). The resulting birnessite in 1 month is so disordered that the elongation and weakening of the diffraction spots make the single-crystal study unsuccessful. Therefore, a longer annealing time is needed. Fortunately, the single-crystal study on an old sample annealed in air for 1 year (**II**) is satisfactory and shows that the buckled layer still exists, although the buckled type changes

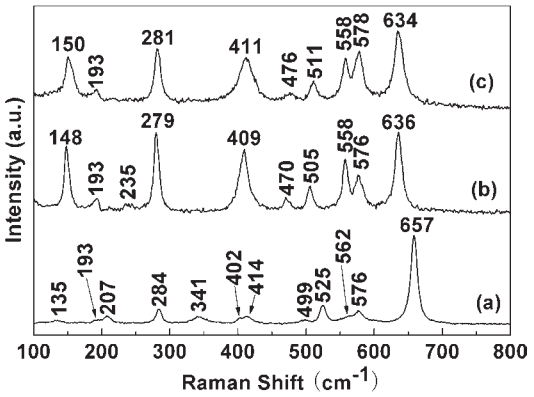

Figure 3. Raman spectra of **I** (a), **II** (b), and synthetic K-birnessite (c), respectively.

to a 2 × 1 buckle. As in **I**, Mn^{3+} and Mn^{4+} reside in Mn(2) and Mn (1) sites in **II**, respectively. The elongation and distortion of $Mn^{3+}O_6$ octahedra were decreased (Figures 1b and 2b). The percentage of Mn^{4+} in **II** was increased, indicating that **I** was oxidized in air.

Because of the layer distortion incorporating large strain in the structure of **I**, it is expected that the Raman scattering of **I** may shift compared with K-birnessite. Figure 3 shows the Raman spectra (excited at 785 nm) of **I**, **II**, and synthetic K-birnessite. The Raman activity of birnessite is low on some reported synthetic samples.[21] However, all samples in this work present high Raman activity with Raman scattering bands in the whole range of 100−800 cm^{-1}. The Raman spectra of synthetic K-birnessite and **II** are basically the same, suggesting they may have similar buckled structures. However, the Raman spectrum of **I** is apparently different, and most of the Raman bands are shifted compared with synthetic K-birnessite. The Raman band at ca. 570 cm^{-1} is the specific fingerprint of the Mn−O vibration along the chains in the manganese dioxide framework.[21] This mode appears at 578 cm^{-1} in K-birnessite, but is observed at 576 cm^{-1} in both **I** and **II**. In another aspect, the Raman band above 600 cm^{-1} can be attributed to the symmetric stretching vibration of MnO_6 groups along the interlayer direction. The frequency of this Mn−O stretching mode at high wavenumber can shift as a function of the interlayer spacing of birnessite, which is related to local lattice distortion. This phenomenon is more obvious here: the frequency is shifted from 634 cm^{-1} in synthetic K-birnessite and 636 cm^{-1} in **II** to 657 cm^{-1} in **I**, corresponding to large lattice distortion of the octahedral layer in **I**.[21]

Buckling of the MnO_6 octahedral layer in birnessite is a result of charge ordering of Mn^{3+}/Mn^{4+} in separate rows and cooperative Jahn−Teller distortion of $Mn^{3+}O_6$ octahedra, which has been recognized in previous studies on EXAFS,[18,20] electron diffraction,[22] or powder XRD data.[5] From the crystallographic point of view, charge ordering of Mn^{3+}/Mn^{4+} will result in two independent Mn sites because of the distinct octahedral environments of Mn^{3+} and Mn^{4+}, as in **I** and **II**. However, structure determinations on the basis of powder XRD data may miss some important structure information, whereas the single-crystal XRD study is powerful.[23] In another aspect, a high degree of disorder of Mn^{3+} and Mn^{4+} within the MnO_6 octahedral layer of birnessite also makes the MnO_6 layer a plane on average. Therefore, the planar and buckled models can be attributed to charge-disordered and -ordered states of Mn^{3+} and Mn^{4+}, respectively. The transformation of **I** to **II** involves a Mn^{3+}/Mn^{4+} order−disorder−order transition.[5] When K-birnessite is

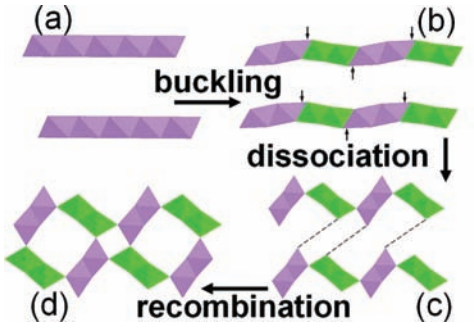

Figure 4. Schematic representation of the hypothesized transformation process of K-birnessite to α-MnO_2 through layer buckling. The crystal structures of planar K-birnessite (a) and **I** (b) looking down the *b* axis, respectively. The small arrows point at the longer Mn(2)−O(1) bonds. (c) Dissociation of the buckled layers. (d) Crystal structure of α-MnO_2 looking down the *c* axis.

calcined in air (around 600 °C)[15,24] or treated in alkaline hydrothermal conditions,[25] it may be converted to α-MnO_2.[26] At a lower KOH/MnO_2 ratio of about 0.25, α-MnO_2 was directly synthesized through a solid-state reaction.[27] Figure 4d shows the crystal structure of α-MnO_2 looking down the *c* axis. It is composed of 2 × 2 tunnels formed by double chains of MnO_6 octahedra.[13] By comparing the crystal structures of birnessite (Figure 4a, ideal planar model), **I**, and α-MnO_2, it is likely that the buckled layer is the intermediate state between birnessite and α-MnO_2. At the beginning of the transformation, water molecules will move out of the layers, while the layers collapse (buckle) in the oxidation process of some Mn^{3+} to Mn^{4+} (or disproportionation of neighboring Mn^{3+} ions to Mn^{4+} and Mn^{2+} ions and subsequent oxidation of Mn^{2+} to Mn^{3+} ions). In this process, the MnO_6 octahedral layer rearrangement may involve a disordered Mn^{3+} aggregate in rows, which decreases the lattice strain and facilitates further the layer-to-tunnel transformation that starts from the breaking of the longer apical Mn−O bond of $Mn^{3+}O_6$ octahedra.[18,28] Further, Figure 4c shows the possible broken layers, which will interconnect again to form the framework of α-MnO_2. Thus, the MnO_6 octahedral buckled layers in **I** can be related to MnO_6 octahedral chains in α-MnO_2. Other types of tunnel structures can be formed in a similar process.

In conclusion, the buckled MnO_6 octahedral layers of **I** and **II** were first successfully stabilized in a HP KOH flux, which gave us a new prospect of the structure of birnessite and the mechanism of layer-to-tunnel transformation.

■ ASSOCIATED CONTENT

Ⓢ Supporting Information. Synthesis and characterization details for **I** and synthetic K-birnessite, index of the powder XRD of synthetic K-birnessite, crystal structure showing the superimposed Mn−O layers for **I**, **II**, and synthetic K-birnessite, respectively, thermal ellipsoid plot and calculated powder XRD for **I** and **II**, respectively, temporal evolution of the powder XRD, TGA, and in situ high-temperature powder XRD for **I**, and a CIF file. This material is available free of charge via the Internet at http://pubs.acs.org.

■ AUTHOR INFORMATION

Corresponding Author
*E-mail: liuxy@jlu.edu.cn. Fax: (+)86-431-85168316.

■ ACKNOWLEDGMENT

This work was supported by the National Natural Science Foundation of China (Grants 20471022 and 40673051).

■ REFERENCES

(1) Talyzin, A. V.; Sundqvist, B.; Szabo, T.; Dekany, I.; Dmitriev, V. *J. Am. Chem. Soc.* **2009**, *131*, 18445.
(2) Lee, Y.; Vogt, T.; Hriljac, J. A.; Parise, J. B.; Hanson, J. C.; Kim, S. J. *Nature* **2002**, *420*, 485.
(3) Loa, I.; Syassen, K.; Kremer, R. K.; Schwarz, U.; Hanfland, M. *Phys. Rev. B* **1999**, *60*, R6945.
(4) Perottoni, C. A.; da Jornada, J. A. H. *Phys. Rev. Lett.* **1997**, *78*, 2991.
(5) Gaillot, A. C.; Lanson, B.; Drits, V. A. *Chem. Mater.* **2005**, *17*, 2959.
(6) Azuma, M.; Yoshida, H.; Saito, T.; Yamada, T.; Takano, M. *J. Am. Chem. Soc.* **2004**, *126*, 8244.
(7) Post, J. E.; Veblen, D. R. *Am. Mineral.* **1990**, *75*, 477.
(8) Lu, Y.; Yang, L.; Wei, M.; Xie, Y.; Liu, T. *J. Solid State Electrochem.* **2007**, *11*, 1157.
(9) Wang, L.; Ebina, Y.; Takada, K.; Kurashima, K.; Sasaki, T. *Adv. Mater.* **2004**, *16*, 1412.
(10) Chen, C. H.; Crisostomo, V. M. B.; Li, W. N.; Xu, L.; Suib, S. L. *J. Am. Chem. Soc.* **2008**, *130*, 14390.
(11) Luo, J.; Zhang, Q.; Huang, A.; Giraldo, O.; Suib, S. L. *Inorg. Chem.* **1999**, *38*, 6106.
(12) Espinal, L.; Suib, S. L.; Rusling, J. F. *J. Am. Chem. Soc.* **2004**, *126*, 7676.
(13) Feng, Q.; Kanoh, H.; Ooi, K. *J. Mater. Chem.* **1999**, *9*, 319.
(14) Beal, E. J.; House, C. H.; Orphan, V. J. *Science* **2009**, *325*, 184.
(15) Chen, R.; Zavalij, P.; Whittingham, M. S. *Chem. Mater.* **1996**, *8*, 1275.
(16) Ma, R.; Bando, Y.; Zhang, L.; Sasaki, T. *Adv. Mater.* **2004** *16*, 918.
(17) Suib, S. L. *Acc. Chem. Res.* **2008**, *41*, 479.
(18) Silvester, E.; Manceau, A.; Drits, V. A. *Am. Mineral.* **1997** *82*, 962.
(19) Crystal data for **I**: $K_{0.66}Mn_2O_4 \cdot 0.28H_2O$ ($K_{1.03}Mn_2O_4$), a = 12.7592(6) Å, b = 2.83850(10) Å, c = 10.4665(5) Å, β = 94.797(3)°, V = 377.74(3) Å^3, Z = 4, M = 214.15 g mol^{-1}, $C2/m$ (No. 12), T = 296(2) K, λ = 0.710 73 Å, D_{calcd} = 3.766 g cm^{-3}, μ = 7.679 mm^{-1}, R1 [$I > 2\sigma(I)$] = 0.0185, and wR2 = 0.0425. Crystal data for **II**: $K_{0.99}Mn_3O_6 \cdot 1.25H_2O$ ($K_{1.39}Mn_3O_6$), a = 14.259(4) Å, b = 2.8438(7) Å, c = 9.526(2) Å, β = 126.908(16)°, V = 308.86(14) Å^3, Z = 2, M = 315.17 g mol^{-1}, $C2/m$ (No. 12), T = 296(2) K, λ = 0.710 73 Å, D_{calcd} = 3.389 g cm^{-3}, μ = 6.938 mm^{-1}, R1 [$I > 2\sigma(I)$] = 0.0397, wR2 = 0.1082.
(20) Ressler, T.; Brock, S. L.; Wong, J.; Suib, S. L. *J. Phys. Chem. B* **1999**, *103*, 6407.
(21) Julien, C.; Massot, M.; Baddour-Hadjean, R.; Franger, S.; Bach, S.; Pereira-Ramos, J. P. *Solid State Ionics* **2003**, *159*, 345.
(22) Liu, Z.; Ma, R.; Ebina, Y.; Takada, K.; Sasaki, T. *Chem. Mater.* **2007**, *19*, 6504.
(23) Chu, Q. X.; Wang, X. F.; Li, Q. L.; Liu, X. Y. *Acta Crystallogr.* **2011**, *C67*, i10.
(24) Chen, C. C.; Golden, D. C.; Dixon, J. B. *Clays Clay Miner.* **1986**, *34*, 565.
(25) Rziha, T.; Gies, H.; Rius, J. *Eur. J. Mineral.* **1996**, *8*, 675.
(26) Thackeray, M. M. *Prog. Solid State Chem.* **1997**, *25*, 1.
(27) Delmas, P. C.; Fouassier, C. *Z. Anorg. Allg. Chem.* **1976** *420*, 184.
(28) Li, Y.; Wu, Y. *Nano Res.* **2009**, *2*, 54.